# 3D Hexagonal Arrangement of DNA Tensegrity Triangles

*Brandon Lu,[1] Simon Vecchioni,[1] Yoel P. Ohayon,[1] Ruojie Sha,[1] Karol Woloszyn,[1] Bena Yang,[1] Chengde Mao,[2] and Nadrian C. Seeman[1*]*

[1]Department of Chemistry, New York University, New York, NY 10003, USA

[2]Department of Chemistry, Purdue University, West Lafayette, Indiana 47907, USA

[*]Address correspondence to this author at ned.seeman@nyu.edu

ABSTRACT. The tensegrity triangle motif utilizes Watson-Crick sticky end cohesion to self-assemble into a rhombohedral crystal lattice using complementary 5′-GA and 5′-TC sticky ends. Here, we report that using non-canonical 5′-AG and 5′-TC sticky ends in otherwise isomorphic tensegrity triangles results in crystal self-assembly in the $P6_3$ hexagonal space group as revealed by X-ray crystallography. In this structure, the DNA double helices bend at the crossover positions, a feature that was not observed in the original design. Instead of propagating linearly, the tilt between base pairs of each right-handed helix results in a left-handed superstructure along the screw axis, forming a microtubule-like structure composed of three double helices with an unbroken channel at the center. This hexagonal lattice has a cavity diameter of 11 nm and a unit cell volume of 886,000 $Å^3$—far larger than the rhombohedral counterpart (5 nm, 330,000 $Å^3$).

**Keywords:** DNA crystals, self-assembly, crystal packing, sticky ends, nanomaterials

The semantic programmability and structural versatility of DNA have been exploited to build various structures on the nanometer scale, from immobile 4-arm junctions[1] to complex 3D objects.[2,3,4] The combination of branched DNA motifs and cohesive sticky ends was used to design the tensegrity triangle motif, which self-assembles into a designer 3D DNA crystal.[5] With three four-arm junctions and seven base-pairs between the crossovers, this motif allows for the DNA

helices to propagate in three linearly-independent directions, resulting in the formation of a rhombohedral 3D crystal lattice.[5] The predictability of Watson-Crick base pairing allowed for the expansion of the tensegrity triangle motif from the original two-turn design containing 21 nucleotide pairs to subsequent designs composed of 31 and 42 nucleotide pairs.[5,6] The robustness of this motif has resulted in modifications to the design with torsionally stressed DNA segments between junctions,[7] multiple triangles per asymmetric unit,[8] and organized semiconductors.[9] Tensegrity triangles have been further used to build DNA walkers used in a molecular assembly line[10] and in reversible, color-changing crystals.[11]

While the sequence of the sticky ends has been studied in great detail through testing Watson-Crick pairing combinations of one, two, three, and four-nucleotide overhangs, as well as the addition of phosphates at the 5' and/or 3' ends of the strands,[12] there have not been studies concerning non-Watson-Crick interactions in the sticky end region. Here, we reverse the order of the sticky end sequence on the helical strand of the tensegrity triangle as shown in Figure 1. Previous attempts to insert modifications inside the motif did not alter the R3 space group when the crystals formed.[13,14] This 3D DNA crystal contains non-Watson-Crick sticky end interactions combined with Watson-Crick base pairing inside each triangle. Sequence information is shown in Table S1 and motif design is shown in Figure S1.

# Results and Discussion

We were able to form needle-shaped crystals that diffracted to 5.68 Å at beamline 17ID at Advanced Photon Source (APS-Argonne National Laboratory, Argonne, IL, USA). Compared to the previously reported rhombohedral-shaped crystals with Watson-Crick sticky end cohesion (Figure 1c), the non-Watson-Crick sticky end resulted in crystals that extend up to 400 μm in

length (Figure 1d). The data integrated in space group $P6_3$ and were solved using molecular replacement with one copy of the original tensegrity triangle (PDB ID: 3GBI) as a search model.[5] Sample X-ray diffraction spots can be found in Figure S2 and 2Fo-Fc and Fo-Fc electron density maps can be found in Figure S3. Unit cell parameters and refinement information can be found in Table 1 with detailed information in Table S2. Accuracy of molecular replacement solution was confirmed using composite omit maps (2mFo-DFc) generated by PHENIX (Figure S4) and cobalt single-wavelength anomalous dispersion (Figure S5). The triangles contain three-fold backbone rotational symmetry, binding to their six neighbors using sticky end cohesion. However, while the rhombohedral triangle propagates linearly, there is an overall bend of $60^o$ in each of the three helices that make up the triangle. Because of the counterclockwise overlapping helices of the tensegrity triangle caused by the three four-arm junctions, each helix of the triangle bending $60^o$ allows the crystals to pack in a hexagonal lattice. This bending of the helices leads to the formation of a left-handed meta helix along the primary screw axis as shown in Figure 2 and Figure S6.

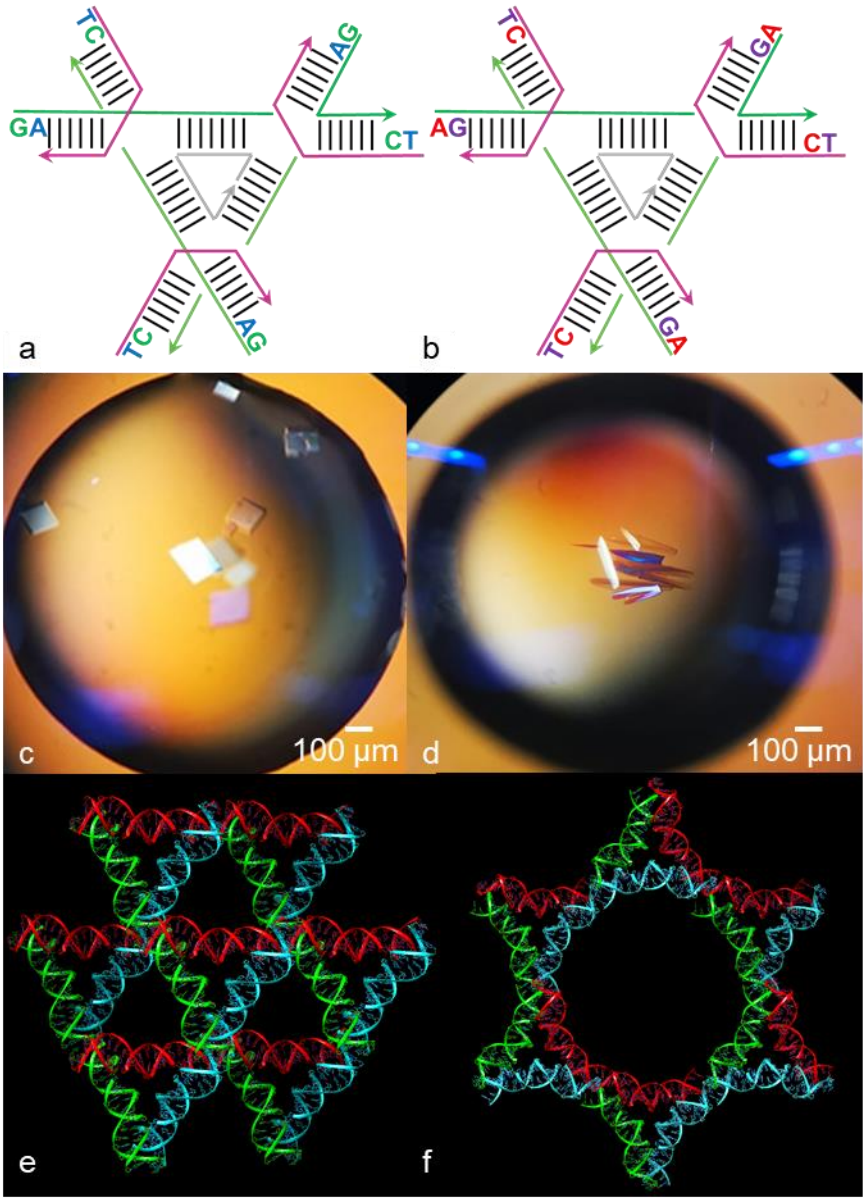


**Figure 1.** Schematic drawings, optical images of crystals, and 3D assembly models of the triangle motifs. **a)** Rhombohedral tensegrity triangle design; **b)** hexagonal tensegrity triangle design. **c)** Crystals in the R3 space group are defined rhombohedra; **d)** while hexagonal crystals extend significantly longer in one dimension, forming a long needle-shaped crystal parallel to the screw axis. Note the straight helices **e)** in the R3 model (PDB ID: 3GBI)[5] and the bent helices **f)** in the $P6_3$ model (PDB ID: 7R96). Contiguous helices share the same color.

| Structure | Hexagonal (PDB ID: 7R96) | Rhombohedral (PDB ID: 3GBI)[5] |
|---|---|---|
| **Resolution** | 5.68 Å | 4.00 Å |
| **Space Group** | $P6_3$ | R3 |
| **Unit Cell Dimensions** | a=b=125.206Å, c=65.277Å, α=β=90°, γ=120° | a=b=c=69.02Å, α = 101.4° |
| **Unit Cell Volume (Å$^3$)** | 885540 | 306211 |
| **$R_{work}$** | 0.1156 | |
| **$R_{free}$** | 0.1549 | |
| **$RSMD_{bonds}$** | 0.008 Å | |
| **$RSMD_{angles}$** | 0.936° | |
| **Clashscore** | 28.975 | |

**Table 1.** X-ray data of hexagonal crystal structure (PDB ID: 7R96).

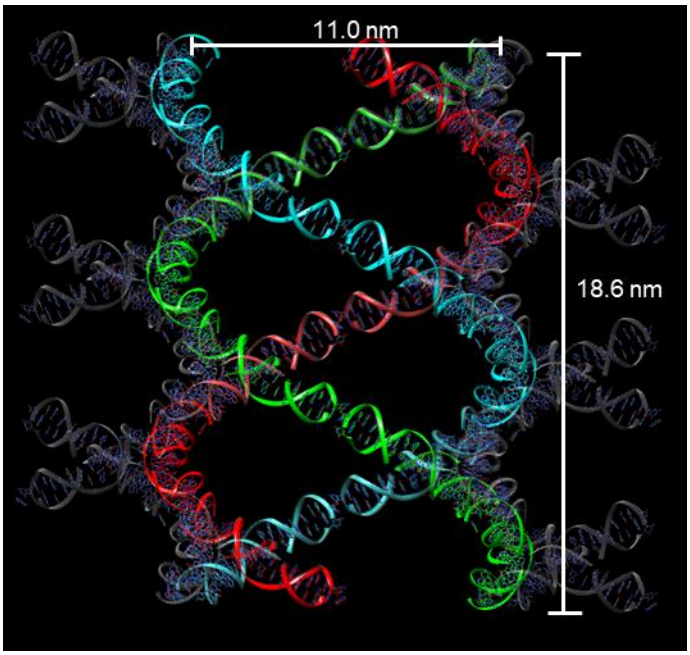


**Figure 2.** One turn of the left-handed triple meta-helix structure, formed along the crystallographic screw axis. The interior of the meta-helix is a continuous channel with a diameter of 11.0 nm. Each constituent duplex of the meta-helix is in a different color. The height of one helical turn of the meta-helix is 18.6 nm.

Unlike previous attempts to use motifs other than the tensegrity triangle, such as the tensegrity square,[15] the minor modification of the sticky ends alone to our original design led to the formation of a crystal structure that contained the same basic unit, the tensegrity triangle, packing in a different space group (Figure 3). While maintaining the triangle's threefold symmetry, the $P6_3$ space group has an arrangement of triangles around the $6_3$ screw axis with a continuous channel that runs parallel with that axis (Figure 3B). This $6_3$ screw axis elucidates the ability for three stacked unit cells to form the triple meta-helix structure shown in Figure 2. There is also an addition of the $2_1$ screw axis between two neighboring triangles, indicating a rotation and translation between triangles. In rhombohedral crystals, neighboring triangles have only translational symmetry which creates continuous straight helices whereas the $2_1$ screw axis in the hexagonal motif allow for the continuous helical turns. Previously, hexagonal 3D DNA lattices have been formed through non-Watson-Crick parallel homopurine interactions resulting in a structure containing non-B-form DNA.[16] This hexagonal structure contained both an antiparallel Watson-Crick region and a parallel homopurine region (GG and AA bases) that allows pairing with adjacent layers of asymmetric units. This structure also contained a large continuous channel through one axis that was used to immobilize enzymes of specific sizes for solid-state catalysis within the DNA framework.[17] Here we kept all the Watson-Crick interactions within the triangle and designed non-Watson-Crick interactions only in the sticky end regions.

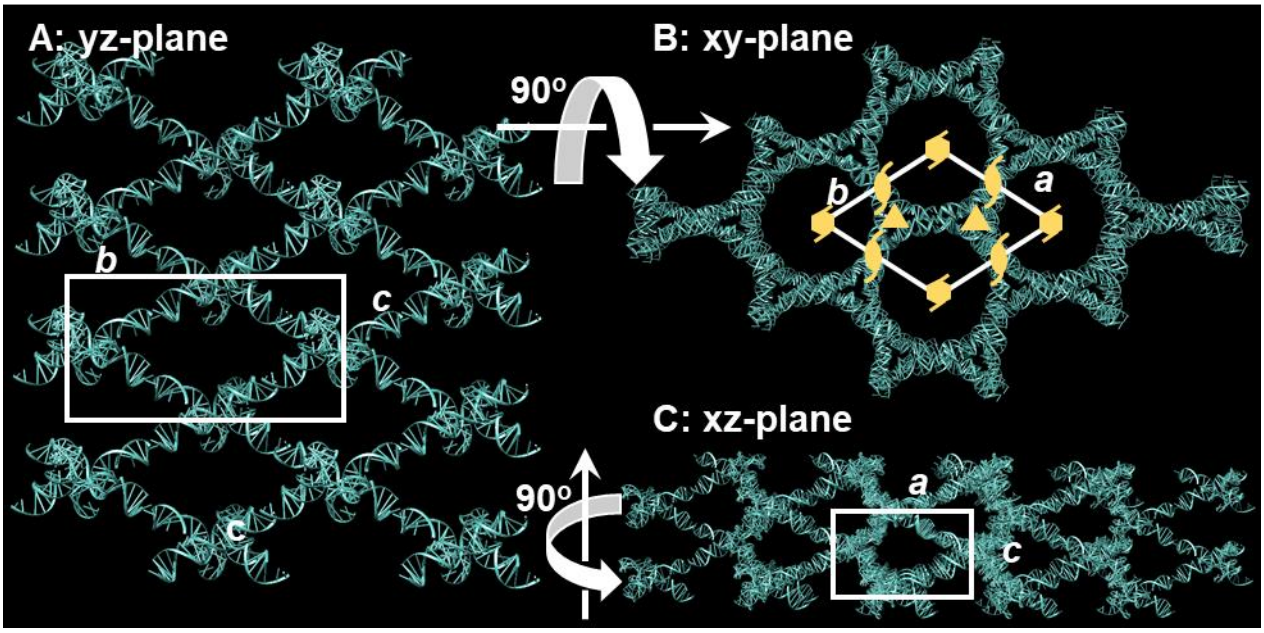


**Figure 3.** Multiple views of crystal packing of hexagonal structure. **A)** A view showing unit cell (white box) with the *b* and *c* dimensions. **B)** A view showing unit cell with *a* and c dimensions with six-fold, three-fold, and two-fold symmetry screw axes. **C)** A view showing unit cell with *a* and *c* dimensions.

The arrangement of six triangles into the hexagonal system rather than the eight in the rhombohedral system led to both a greater cross-sectional area (9500 $Å^2$ vs. 2300 $Å^2$)[5] and a larger cavity size (470,000 $Å^3$ vs. 103,000 $Å^3$) with parameters estimated by subtracting two radii of the double helix from the unit cell parameters.[5] Measurements and calculations of these values for the hexagonal structure are shown in Figure S7. Additionally, there is a continuous channel through the middle of the hexagon which propagates throughout the crystal. The unique, left-handed, triple meta-helix found in the crystal structure is an interesting observation of a higher order structure self-assembling within a 3D DNA crystal (Figure S8). Stereoscopic views of a triangle with its six sticky end partners can be seen in Figure S9 with views from the top and side. As with the

rhombohedral structure, each triangle connects to six other triangles *via* sticky end cohesion, but the bend in the helix causes the sticky end partners to stack vertically, which results in triangles going in an "up" and "down" pattern (Figure S9C). The resulting arrangement can be seen in Figure 3A. Other meta-structures have been formed using combinations of large assemblies of 2D DNA, which have exhibited limited success when translated into 3D nanostructures.[18]

*Tilt of the base pairs*

Large differences in the tilt of the base pairs are observed in the four-arm junction region, unlike in the rhombohedral lattice using the webserver Web 3DNA 2.0. as seen in Table S3.[19] The tilt measures the rotation of the base pair step about the x-axis, indicating an axial bend in the helix.[19] We see that the crossover positions in both structures have significant tilt and differences in those tilts contribute to the overall tilt in the hexagonal motif (base pair steps 5, 6, 12, and 13 in Table S3). This observation conforms with the expectation that the immobile junction reported in 1983 forms the characteristic stacked "H" shape rather than a cross-like motif.[20] However, the large variation in bending for the junction found in the hexagonal motif is a surprising discovery, since branched junctions have specific angles that they favor, which has been exploited by others to prescribe certain crystal structures.[21] We also see significant tilt differences at other locations in the structure and at the sticky end, as shown in Table S3.

The polarity of the sticky end sequences was reversed so that an adenine would face a cytosine and a guanine would face a thymine. Guanine and thymine are known to form a "wobble" base pair[22] with different glycosyl angles compared to canonical Watson-Crick base pairing.[23] The G:T pair results in structures adopting noncanonical conformations.[24] However, adenine and cytosine are fully mismatched, and are not expected to form a base pair.[25] The double helices in our modified triangle adopt a B-form conformation as shown by CD spectroscopy (Figure S10) similar

to the spectrum of the original tensegrity triangle.[26] Because of the non-canonical nature of the sticky end region, it is likely that the interactions between triangle units are significantly weaker than in prior tensegrity triangle motifs. Extrapolating this further lends credence to the idea that base-stacking can guide the formation of 3D crystals similar to those in 1D and 2D DNA arrays[27] as well as on lipid surfaces.[28] The possibility for DNA base-stacking alone to drive the self-assembly of tensegrity triangles ("blunt-end cohering crystals") has been explored in prior studies but did not yield 3D crystals.[12] As such, stronger and/or more specific interactions between tensegrity triangle units may be needed in order to form 3D crystals compared to 2D and 1D structures. This suggests that the G:T wobble base pair in our motif is necessary to drive the self-assembly of the hexagonal lattice, as it is unlikely the A and C bases are contributing significantly to the sticky end interaction.

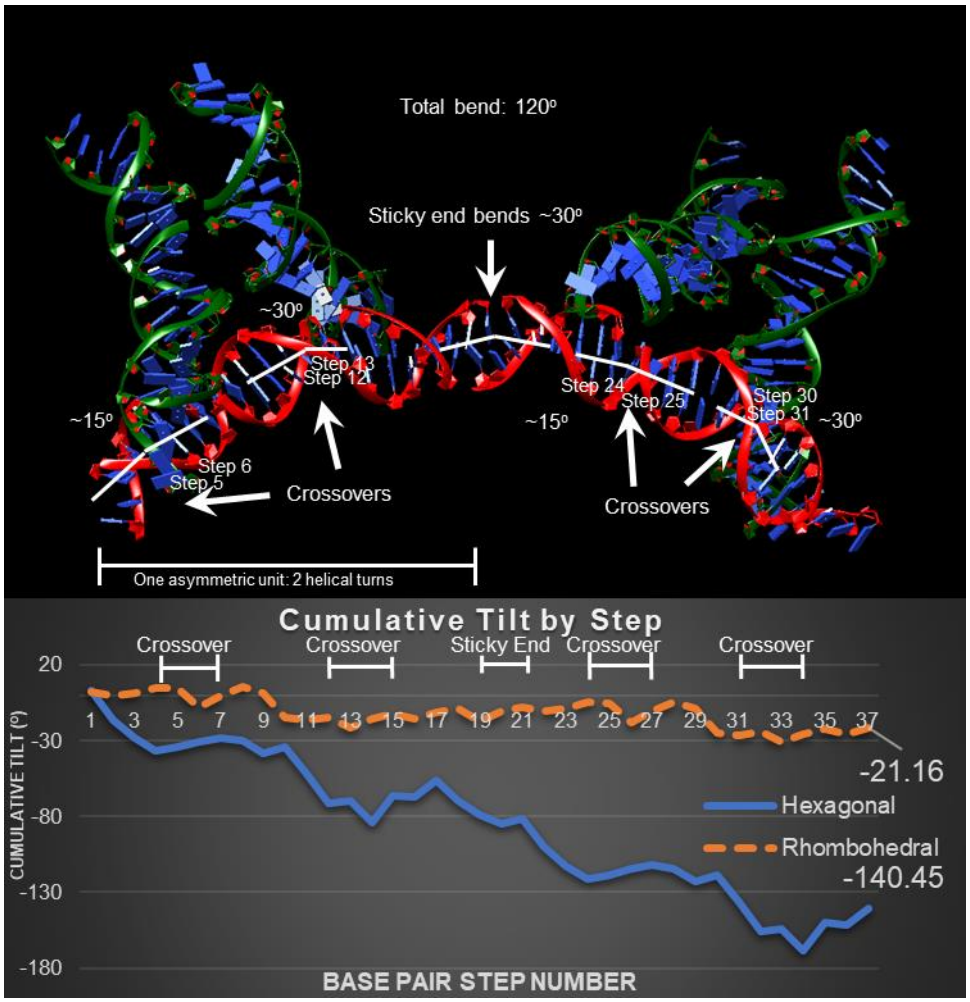


**Figure 4.** Junction bending in two asymmetric units. *Top:* Two asymmetric units of the hexagonal tensegrity triangle motif with bending angles labeled. Crossovers are indicated and degree of tilt is labeled. Helical step numbering is shown for crossover region. There is a $2_1$ screw axis in between the two triangles so that triangles are slightly rotated with respect to its sticky end neighbor (in comparison to straight triangles in the rhombohedral motif). *Bottom:* Cumulative base pair tilt with helical steps numbered. Data plotted from Table S3 and calculated by Web 3 DNA 2.0. Total difference in tilt between rhombohedral and hexagonal structures across two asymmetric units is about 120°, forming the base unit of a hexagon.

As shown in Figure 4, the bending primarily occurs at the crossover regions. Since canonical tensegrity triangle crystals form straight helices and altering only the sticky end sequence results in the tilted hexagonal lattice, it is likely that the sticky end sequence drives the global geometric alteration. Past studies have shown that bending can be induced in the crossover regions in DNA origami helix bundles by building stresses into the helices to cause strain.[29] Additionally, it was found that crossover regions require less force to bend than B-form DNA, which helps explain the tilt differences at the crossover regions.[29] Our structure confirms this effect in a self-assembling 3D DNA crystal, as the stresses caused by the non-canonical sticky end region result in tilt at the crossover regions. The sticky ends also contribute to some degree in the bending of the helix, which introduce nicks between motifs. Nicks in the DNA double helix can absorb flexible defects and relax the bending elsewhere in the structure.[30] The propensity to bend occurs mainly within stressed DNA, indicating that the non-Watson-Crick interactions at the sticky end induce stress in the double helix.[31] As such, both the crossover regions and the nicks at the sticky end appear to absorb the non-canonical geometry of the sticky ends, causing the bend in the helix that results in hexagonal arrangement of triangular subunits.

# Conclusions

In summary, we demonstrate the ability for the DNA tensegrity triangle to self-assemble in the hexagonal $P6_3$ space group. This behavior underscores the ability of a simple motif to crystallize in different space groups based on sticky end sequence i.e. the information contained in the oligonucleotide sequence. We observe that non-canonical interactions in sticky ends have a profound effect on local geometry, altering the global topology during crystal self-assembly. Future work will pursue additional motifs that can form in the hexagonal lattice and probe the

underlying mechanics of this self-assembly pathway. The larger space inside this motif may also be used for the incorporation of larger guest molecules and nanomaterials.

# Methods

## DNA Synthesis and Purification

Strands were ordered from Integrated DNA Technologies with standard desalting. DNA oligomers were then purified using denaturing polyacrylamide gel electrophoresis containing 20% acrylamide (19:1 acrylamide:bisacrylamide), TBE buffer (40 mM Tris, 40 mM boric acid, 2 mM EDTA), and 50% by mass urea running at 600V for 1 hour. Gels were stained with ethidium bromide and bands corresponding to the expected size of strands were excised under UV illumination. DNA was eluted in buffer solution containing 500 mM ammonium acetate, 10 mM magnesium acetate, and 1 mM EDTA at 4 $^{o}$C for one day. Eluate was extracted with 1-butanol to remove ethidium bromide, and DNA was recovered by ethanol precipitation. Concentration of DNA in final solution was estimated with OD at 260 nm using an IMPLEN P300 Nanophotometer (München, DE).

## Crystallization

Crystals were grown from 5 μL hanging drops at pH 9.5 containing 6 μM DNA, 40 mM Tris, 20 mM acetic acid, 2 mM EDTA, 583 mM ammonium sulfate, 0.25 mM cobalt hexammine, and 12.5 mM magnesium acetate equilibrated against a 600 μL reservoir containing buffer solution with 120 mM Tris, 6 mM EDTA, 60 mM acetic acid, 37.5 mM magnesium acetate, and 1.75 M ammonium sulfate. Crystal trays were placed in a thermally controlled incubator and slow annealed from 60$^{o}$C to 20 °C with a cooling rate of 0.4 °C per hour. Crystals were then transferred to cryosolvent containing 70% of the buffer solution of the crystal reservoir and 30% glycerol. Crystals were then frozen by immersion in liquid nitrogen and shipped for X-ray diffraction.

### Data Collection and Structure Solution

X-Ray diffraction data were collected on beamline 17ID at Advanced Photon Source, Argonne National Laboratory at 1.60648 Å near the cobalt K-edge. The diffraction data were processed using the automatic data processing package autoPROC (Global Phasing, Cambridge, UK), which automatically indexes the data for space group determination, integrates the data in the space group using XDS, and scales the data using AIMLESS.[32] Results from X-ray diffraction were processed for isotropy using the STARANISO server (Global Phasing) to remove directional dependence of the resolution, allowing for an ellipsoidal resolution cutoff which increases the limit for these crystals by about 1-2 Å.[33] Structures were solved using molecular replacement (search model PDB ID: 3GBI), and accuracy of solution was confirmed using cobalt single wavelength anomalous dispersion *via* the PHENIX program package.[34] The Coot program[35] and UCSF Chimera[36] were used to model crystal structures and create figures.

## Conflicts of Interest

There are no conflicts of interest to declare.

## Supporting Information

Sequence information; full sequence schematic; X-ray diffraction spots; X-ray refinement data; Fo-Fc and 2Fo-Fc electron density maps; composite omit maps; phased electron density maps; stereoscopic views of triple meta-helix; cross-sectional area and cavity size calculations; 3D printed model of triple meta-helix; Base pair tilt table; additional representation of triangle connected to neighbors; circular dichroism spectrum.

# Acknowledgements

We acknowledge support of the following grants to N.C.S.: N000141912596 from the Office of Naval Research, DE-SC0007991 from the Department of Energy, 2106790 from the National Science Foundation, RPG0010/2017 from Human Frontiers Science Program, DMR-1420073 from the MRSEC Program of the National Science Foundation. Partial support given to B.L. through the Société de Chimie Industrielle Undergraduate Fellowship.

# References


1 Seeman, N. C. Nucleic Acid Junctions and Lattices. *J Theor Biol* **99**, 237-247, doi:10.1016/0022-5193(82)90002-9 (1982).

2 Chen, J. H. & Seeman, N. C. Synthesis from DNA of a Molecule with the Connectivity of a Cube. *Nature* **350**, 631-633, doi:10.1038/350631a0 (1991).

3 Wang, W., Chen, S., An, B., Huang, K., Bai, T., Xu, M., Bellot, G., Ke, Y., Xiang, Y. & Wei, B. Complex Wireframe DNA Nanostructures from Simple Building Blocks. *Nat Commun* **10**, 1067, doi:10.1038/s41467-019-08647-7 (2019).

4 He, Y., Tian, Y., Ribbe, A. E. & Mao, C. Highly Connected Two-Dimensional Crystals of DNA Six-Point-Stars. *J Am Chem Soc* **128**, 15978-15979, doi:10.1021/ja0665141 (2006).

5 Zheng, J., Birktoft, J. J., Chen, Y., Wang, T., Sha, R., Constantinou, P. E., Ginell, S. L., Mao, C. & Seeman, N. C. From Molecular to Macroscopic *Via* the Rational Design of a Self-Assembled 3D DNA Crystal. *Nature* **461**, 74-77, doi:10.1038/nature08274 (2009).

6 Nguyen, N., Birktoft, J. J., Sha, R., Wang, T., Zheng, J., Constantinou, P. E., Ginell, S. L., Chen, Y., Mao, C. & Seeman, N. C. The Absence of Tertiary Interactions in a Self-Assembled DNA Crystal Structure. *J Mol Recognit* **25**, 234-237, doi:10.1002/jmr.2183 (2012).

7 Hernandez, C., Birktoft, J. J., Ohayon, Y. P., Chandrasekaran, A. R., Abdallah, H., Sha, R., Stojanoff, V., Mao, C. & Seeman, N. C. Self-Assembly of 3D DNA Crystals Containing a Torsionally Stressed Component. *Cell Chem Biol* **24**, 1401-1406 e1402, doi:10.1016/j.chembiol.2017.08.018 (2017).

8 Wang, T., Sha, R., Birktoft, J., Zheng, J., Mao, C. & Seeman, N. C. A DNA Crystal Designed to Contain Two Molecules Per Asymmetric Unit. *J Am Chem Soc* **132**, 15471-15473, doi:10.1021/ja104833t (2010).

9 Wang, X., Sha, R., Kristiansen, M., Hernandez, C., Hao, Y., Mao, C., Canary, J. W. & Seeman, N. C. An Organic Semiconductor Organized into 3D DNA Arrays by "Bottom-up" Rational Design. *Angew Chem Int Ed Engl* **56**, 6445-6448, doi:10.1002/anie.201700462 (2017).

10 Gu, H., Chao, J., Xiao, S. J. & Seeman, N. C. A Proximity-Based Programmable DNA Nanoscale Assembly Line. *Nature* **465**, 202-205, doi:10.1038/nature09026 (2010).

11 Hao, Y., Kristiansen, M., Sha, R., Birktoft, J. J., Hernandez, C., Mao, C. & Seeman, N. C. A Device That Operates within a Self-Assembled 3D DNA Crystal. *Nat Chem* **9**, 824-827, doi:10.1038/nchem.2745 (2017).

12 Ohayon, Y. P., Hernandez, C., Chandrasekaran, A. R., Wang, X., Abdallah, H. O., Jong, M. A., Mohsen, M. G., Sha, R., Birktoft, J. J., Lukeman, P. S., Chaikin, P. M., Ginell, S. L., Mao, C. & Seeman, N. C. Designing Higher Resolution Self-Assembled 3D DNA Crystals *Via* Strand Terminus Modifications. *ACS Nano* **13**, 7957-7965, doi:10.1021/acsnano.9b02430 (2019).

13 Stahl, E., Praetorius, F., de Oliveira Mann, C. C., Hopfner, K. P. & Dietz, H. Impact of Heterogeneity and Lattice Bond Strength on DNA Triangle Crystal Growth. *ACS Nano* **10**, 9156-9164, doi:10.1021/acsnano.6b04787 (2016).

14 Satange, R., Chang, C. K. & Hou, M. H. A Survey of Recent Unusual High-Resolution DNA Structures Provoked by Mismatches, Repeats and Ligand Binding. *Nucleic Acids Res* **46**, 6416-6434, doi:10.1093/nar/gky561 (2018).
15 Simmons, C. R., Zhang, F., Birktoft, J. J., Qi, X., Han, D., Liu, Y., Sha, R., Abdallah, H. O., Hernandez, C., Ohayon, Y. P., Seeman, N. C. & Yan, H. Construction and Structure Determination of a Three-Dimensional DNA Crystal. *J Am Chem Soc* **138**, 10047-10054, doi:10.1021/jacs.6b06508 (2016).
16 Paukstelis, P. J., Nowakowski, J., Birktoft, J. J. & Seeman, N. C. Crystal Structure of a Continuous Three-Dimensional DNA Lattice. *Chem Biol* **11**, 1119-1126, doi:10.1016/j.chembiol.2004.05.021 (2004).
17 Geng, C. & Paukstelis, P. J. DNA Crystals as Vehicles for Biocatalysis. *J Am Chem Soc* **136**, 7817-7820, doi:10.1021/ja502356m (2014).
18 Yao, G., Zhang, F., Wang, F., Peng, T., Liu, H., Poppleton, E., Sulc, P., Jiang, S., Liu, L., Gong, C., Jing, X., Liu, X., Wang, L., Liu, Y., Fan, C. & Yan, H. Meta-DNA Structures. *Nat Chem* **12**, 1067-1075, doi:10.1038/s41557-020-0539-8 (2020).
19 Li, S., Olson, W. K. & Lu, X. J. Web 3DNA 2.0 for the Analysis, Visualization, and Modeling of 3D Nucleic Acid Structures. *Nucleic Acids Res* **47**, W26-W34, doi:10.1093/nar/gkz394 (2019).
20 Carpenter, M. L., Lowe, G. & Cook, P. R. The Structure of 4-Way DNA Junctions: Specific Binding of Bis-Intercalators with Rigid Linkers. *Nucleic Acids Res* **24**, 1594-1601, doi:10.1093/nar/24.9.1594 (1996).
21 Simmons, C. R., MacCulloch, T., Zhang, F., Liu, Y., Stephanopoulos, N. & Yan, H. A Self-Assembled Rhombohedral DNA Crystal Scaffold with Tunable Cavity Sizes and High-Resolution Structural Detail. *Angew Chem Int Ed Engl* **59**, 18619-18626, doi:10.1002/anie.202005505 (2020).
22 Imhof, P. & Zahran, M. The Effect of a G:T Mispair on the Dynamics of DNA. *PLoS One* **8**, e53305, doi:10.1371/journal.pone.0053305 (2013).
23 Varani, G. & McClain, W. H. The G X U Wobble Base Pair. A Fundamental Building Block of Rna Structure Crucial to Rna Function in Diverse Biological Systems. *EMBO Rep* **1**, 18-23, doi:10.1093/embo-reports/kvd001 (2000).
24 Rangadurai, A., Szymanski, E. S., Kimsey, I., Shi, H. & Al-Hashimi, H. M. Probing Conformational Transitions Towards Mutagenic Watson-Crick-Like G.T Mismatches Using Off-Resonance Sugar Carbon R1rho Relaxation Dispersion. *J Biomol NMR* **74**, 457-471, doi:10.1007/s10858-020-00337-7 (2020).
25 Seela, F. & Budow, S. Mismatch Formation in Solution and on DNA Microarrays: How Modified Nucleosides Can Overcome Shortcomings of Imperfect Hybridization Caused by Oligonucleotide Composition and Base Pairing. *Mol Biosyst* **4**, 232-245, doi:10.1039/b713259j (2008).
26 Chandrasekaran, A. R., Mathivanan, J., Ebrahimi, P., Vilcapoma, J., Chen, A. A., Halvorsen, K. & Sheng, J. Hybrid DNA/Rna Nanostructures with 2'-5' Linkages. *Nanoscale* **12**, 21583-21590, doi:10.1039/d0nr05846g (2020).
27 Woo, S. & Rothemund, P. W. Self-Assembly of Two-Dimensional DNA Origami Lattices Using Cation-Controlled Surface Diffusion. *Nat Commun* **5**, 4889, doi:10.1038/ncomms5889 (2014).

28 Suzuki, Y., Endo, M. & Sugiyama, H. Lipid-Bilayer-Assisted Two-Dimensional Self-Assembly of DNA Origami Nanostructures. *Nat Commun* **6**, 8052, doi:10.1038/ncomms9052 (2015).
29 Dietz, H., Douglas, S. M. & Shih, W. M. Folding DNA into Twisted and Curved Nanoscale Shapes. *Science* **325**, 725-730, doi:10.1126/science.1174251 (2009).
30 Cong, P., Dai, L., Chen, H., van der Maarel, J. R., Doyle, P. S. & Yan, J. Revisiting the Anomalous Bending Elasticity of Sharply Bent DNA. *Biophys J* **109**, 2338-2351, doi:10.1016/j.bpj.2015.10.016 (2015).
31 Vologodskii, A. & Frank-Kamenetskii, M. D. Strong Bending of the DNA Double Helix. *Nucleic Acids Res* **41**, 6785-6792, doi:10.1093/nar/gkt396 (2013).
32 Vonrhein, C., Flensburg, C., Keller, P., Sharff, A., Smart, O., Paciorek, W., Womack, T. & Bricogne, G. Data Processing and Analysis with the Autoproc Toolbox. *Acta Crystallogr D Biol Crystallogr* **67**, 293-302, doi:10.1107/S0907444911007773 (2011).
33 Tickle, I. J., Flensburg, C., Keller, P., Paciorek, W., Sharff, A., Vonrhein, C. & Bricogne, G. *Staraniso*, 2018).
34 Adams, P. D., Afonine, P. V., Bunkoczi, G., Chen, V. B., Davis, I. W., Echols, N., Headd, J. J., Hung, L. W., Kapral, G. J., Grosse-Kunstleve, R. W., McCoy, A. J., Moriarty, N. W., Oeffner, R., Read, R. J., Richardson, D. C., Richardson, J. S., Terwilliger, T. C. & Zwart, P. H. Phenix: A Comprehensive Python-Based System for Macromolecular Structure Solution. *Acta Crystallogr D Biol Crystallogr* **66**, 213-221, doi:10.1107/S0907444909052925 (2010).
35 Emsley, P., Lohkamp, B., Scott, W. G. & Cowtan, K. Features and Development of Coot. *Acta Crystallogr D Biol Crystallogr* **66**, 486-501, doi:10.1107/S0907444910007493 (2010).
36 Pettersen, E. F., Goddard, T. D., Huang, C. C., Couch, G. S., Greenblatt, D. M., Meng, E. C. & Ferrin, T. E. Ucsf Chimera--a Visualization System for Exploratory Research and Analysis. *J Comput Chem* **25**, 1605-1612, doi:10.1002/jcc.20084 (2004).

For Table of Contents Only